Additive Manufacturing 42 (2021) 102001

Contents lists available at ScienceDirect

Additive Manufacturing

journal homepage: www.elsevier.com/locate/addma

In-situ monitoring of deformation in rapid prototyped injection molds

Sz. Krizsma [a], N.K. Kovács [a], J.G. Kovács [a,b,*], A. Suplicz [a]

[a] Department of Polymer Engineering, Faculty of Mechanical Engineering, Budapest University of Technology and Economics, Műegyetem rkp. 3., H-1111 Budapest, Hungary

[b] MTA-BME Lendület Lightweight Polymer Composites Research Group, Műegyetem rkp. 3., H-1111 Budapest, Hungary

ARTICLE INFO

Keywords:
Rapid prototyping
Rapid tooling
Injection molding
3D printing
PolyJet technology

ABSTRACT

The ever growing demand for reducing costs and decreasing the time to market in today's plastics industry makes rapid tooling and rapid prototyping a highly researched area. 3D printed injection mold inserts make it possible to produce prototype parts in small series fast and cost-effectively. The mechanical strength and therefore the life expectancy of 3D printed polymeric injection mold inserts are low compared to their traditional steel counterparts. In order to increase the reliability and life expectancy of polymeric mold inserts, in-situ state monitoring during injection molding is essential. In this paper, we analyse the effect of thermal and mechanical loads on the resulting strains of the mold inserts. Three series of rectangular plate products were injection molded with a different type of insert in each series. The pressure inside the cavity and the strain of the 3D printed inserts were measured during injection molding. We correlated maximal cavity pressures and changes in strain with each other in order to set up the deformation characteristic of the inserts. The results indicate a satisfactory correlation between the maximal cavity pressures and the strain change of the inserts. The second important result was that strain gauges can be applied to in-situ monitor the state of the inserts during injection molding.

1. Introduction

In today's plastics processing industry, the drive to reduce the time to market and the appearance of novel additive manufacturing technologies like 3D printing, bring rapid tooling into the focus of researchers and industry alike [1]. The application of 3D printed mold inserts is a promising area of research. 3D printing allows the production of parts in a wide range of geometries, giving freedom to design engineers. In large series production, 3D printed metal inserts made by direct metal laser sintering (DMLS) are an alternative to traditional injection molds [2]. For the production of small series, polymer mold inserts can be used. They are typically made by selective laser sintering (SLS), stereolitography (SLA) or PolyJet technology [3,4]. Several case studies have been made to prove the in-mold applicability of additively manufactured inserts.

Researchers prove the applicability of additively manufactured injection molds and mold inserts with a series of laboratory-scale case studies. León-Cabezas et al. [5] prepared injection mold prototypes by 3D printing (PolyJet technology) from ABS-like photopolymerisation resin and by other technologies. The materials used for injection molding were elastomeric polyethylene, polypropylene and ABS. The authors produced two different types of molds, one for tensile test specimens and one for a spinning top toy. The spinning top mold endured 20 injection molding cycles altogether, while the tensile test specimen mold cracked after 12 cycles. Whlean et al. [6] created a master unit die from aluminum by machining. This die was used to house the mold inserts which were produced from high temperature (HT) resin by SLA. The product made with this mold was a tweezer-like clip, and after 20 shots, the mold insert began to fracture. Ali et al. [7] created additively manufactured mold inserts by vat-based photopolymerisation. The injection molded material was ABS and they used two unaged and four aged inserts. During injection molding, they detected the locations of the cracks and measured the cycle numbers corresponding to crack initiation and the critical failure of the inserts. The unaged inserts showed crack initiation after 70 and 95 cycles and critical failure occurred at 110 and 143 cycles, respectively. In the case of the aged inserts, initial cracks occurred at 50, 30, 8 and 12 cycles and failure happened at 110, 85, 35 and 45 cycles, respectively. These results indicate that first, these mold inserts are for small series applications and second, that thermal aging has a negative effect on the life expectancy of

* Corresponding author at: Department of Polymer Engineering, Faculty of Mechanical Engineering, Budapest University of Technology and Economics, Műegyetem rkp. 3., H-1111 Budapest, Hungary.
E-mail address: kovacs@pt.bme.hu (J.G. Kovács).

https://doi.org/10.1016/j.addma.2021.102001
Received 11 January 2021; Received in revised form 12 March 2021; Accepted 3 April 2021
Available online 20 April 2021

the inserts. Cheah et al. [8] used an indirect rapid soft tooling approach to produce a mobile telephone front housing. In their workflow, they first fabricated a master pattern, using SLA, then they casted aluminum-filled epoxy resin around the master pattern to create the cavity and then the core half of the mold. After the proper curing of the resin, they machined it to reach the required dimensional accuracy and surface quality. They used the inserts to produce two series of parts. First, they used a PC/ABS resin and managed to reach 200 cycles without significant tool wear. Second, they used a PC grade and observed a crack line on the cavity side of the mold after 400 cycles.

As can be seen from the previous results, the application of mold inserts made by additive manufacturing is a new and feasible route. With the use of 3D printing technologies, mold inserts can be produced with conformal cooling channels. This is an intensively researched area because conformal cooling channels reduce cycle time and increase productivity [9,10]. Park et al. [11] applied 3D printed metal inserts made by selective laser melting (SLM) to reduce the cooling time of geometrically complex segments of an automotive part. The design of these AM inserts was supported by injection molding simulations. Conformal cooling channels reduced cycle time by approximately 30% compared to conventional cooling. Another advantage of conformal cooling was the improvement of surface quality in areas of interest. Brooks et al. [12] compared the effectiveness of conventional and conformal cooling channels with the concept of conformal cooling layers they introduced. They demonstrated the advantages of conformal cooling methods compared to conventional cooling channels by simulation. The application for conformal cooling is not limited to injection molding only. Au et al. [13] demonstrated the effectiveness of conformal cooling channels by injection molding simulation in the case of a plastic bottle blow molding. *Tomasoni* et al. [14] applied topology optimization for the design of a conformal cooling layout of a thermoforming mold. *Wu* et al. [15] created a finite element-based optimization approach for designing conformal cooling. The resulting geometries can be manufactured by 3D printing: SLA or powder bed fusion (PBF).

Prototype molds also appear in specific injection molding applications [16]. *Kalami* et al. [17] created a low-volume injection mold for the production of a cable bundle by overmolding. They applied a hybrid mold fabrication methodology, where they extruded a sacrificial product-shaped pattern. Then, they used this pattern to produce a resin-based insert, which was then inserted into a metal mold base frame. As another special field of application Vaezi et al. [18] made a case study, in which they first injection molded wax patterns into an aluminum-filled epoxy resin mold, then coated the wax pattern with ceramics, then removed the wax and finally they produced gas turbine blades using the ceramic shells. For the injection molding of wax patterns, they used rapid tooling (RT) technologies, namely epoxy resin tooling and silicon rubber molding. Their conclusion was that the application of EP resin molds is a new and cost-effective solution for the small batch production of gas turbine blades.

Several comparative studies of polymeric and metallic injection molds were carried out in the literature. Jahan et al. [19] introduced a coupled thermal–fluid topology optimization algorithm for the design of conformal cooling channels. They made a case study, which included the design and simulation of the mold core, manufacturing by metal 3D printing, heat treatment and finishing, and injection molding with the mold. They compared the cooling performance of the machined core and the AM core and found that the AM core is capable of manufacturing plastic products in an industrial environment. The AM cores can be an alternative to traditional machined cores when made from powders with the proper thermal conductivity and other thermomechanical properties. Hopkinson et al. [20] compared two aluminum injection mold core inserts with rough and smooth surfaces with a core insert made by stereolitography. They compared ejection forces, heat transfer through the inserts and the surface roughness of the product. All molds were able to produce over 50 polypropylene parts without any sign of damage to either the tool or the part. Their first conclusion was that lower values of processing parameters (clamping force, injection speed and injection pressure) are needed for the SL cores to avoid mechanical failure. Second, they found that average surface roughness did not change significantly, indicating that tool wear is negligible in small series production. Third, in line with their expectations, the higher surface roughness in the case of the SL tool and the rough aluminum tool resulted in higher ejection forces. Fourth, the significantly worse thermal conductivity of the SL mold increased cycle time as the mold needed extra cooling time after the part was ejected. Mendible et al. [21] created a comparative study of injection mold inserts made by additive and traditional manufacturing technologies. They produced a 3D printed polymer insert from Digital ABS using PolyJet technology, a bronze insert by DMLS and a machined stainless steel insert. They found that the behavior of the bronze and the stainless steel inserts and the quality of the products injection molded with them were similar and that both inserts endured 500 cycles without any signs of failure. The PolyJet insert started producing defective parts after 80 cycles and failure occurred at 116 cycles. Another result was that the PolyJet inserts cooled more slowly, which increased the shrinkage and crystallinity of the molded products. Kampker et al. [22] manufactured three mold inserts for the production of tensile test specimens. They also produced Charpy impact test specimens. These inserts were made of aluminum (by traditional machining), Digital ABS (by PolyJet technology) and PA 3200 GF (by SLS). They found significant differences in the mechanical properties of the test specimens, especially in break elongation. The break elongation of the tensile test specimens made with the polymer tools was significantly lower compared to the specimens produced with the aluminum tool. The authors claimed that a possible explanation of this embrittlement was the different morphological structure of the specimens caused by the lower thermal conductivity and the higher surface roughness of the polymer molds. Tábi et al. [23] compared the thermal, mechanical and thermomechanical properties of injection molded PLA plates produced by a conventional steel mold and a PolyJet mold insert. The plates produced with the PolyJet insert showed significantly higher crystallinity compared to the ones made with the steel mold. The difference in crystallinity is mainly due to the low thermal conductivity of the PolyJet mold and the resulting longer cooling time.

Dimensional accuracy is a primary concern in the injection molding industry. Martinho et al. [24] created a hybrid mold with interchangeable blocks, produced by traditional machining and rapid tooling techniques. They analysed the effect of different core and cavity material combinations (epoxy resin composite and steel) among others, on shrinkage. They found that the shrinkage of the parts increased when the resin cores were used, which was partly due to the deformation of the resin core caused by the injection pressure. Harris et al. [25] compared the shrinkage characteristics of injection molded parts made with two mold inserts of different geometries. The inserts were produced by SLA from a commercially available resin, and by machining from aluminum. The parts were injection molded from PA66 and ABS. They found that the PA66 shrank twice as much when injection molded in an SL tool as in an aluminum tool. On the other hand, they found no such difference in the shrinkage of the ABS parts. They also demonstrated the effect of the thermal expansion of the plastic tools on the shrinkage of the final products.

The conclusion of the literature review is that polymeric mold inserts are currently only suitable for small series and prototype production due to their low mechanical strength and stiffness compared to metallic inserts. Because of these limited mechanical properties, the processing parameters of injection molding have to be carefully adjusted. The applicable holding pressure is low, therefore the compensation of part shrinkage is limited. In the literature, we did not find research articles discussing comprehensive in-situ and real-time state monitoring of 3D printed mold inserts during injection molding. In the present research article, our goal is to lay the foundations of a new in-situ temperature and strain state monitoring method for mold inserts. By this continuous state monitoring the life expectancy of the inserts can be increased and

the processing parameters can be adjusted more precisely.

2. Materials and methods

2.1. The applied mold and the mold inserts

Additively manufactured mold inserts were employed and strain was measured at the back of the inserts. The location of the strain gauge, and the dimensions of the mold insert can be seen in Fig. 1. A rectangular cut-out (10 mm × 7 mm x 2 mm) was prepared at the back of the insert for the wires connected to the strain gauge. The strain gauge was *HBM 1-LY11–3/350* and its data was collected by a *Spider 8* unit. Cavity pressure was directly measured with a *Kistler 6182 B* pressure sensor and its data was collected by a *Como Injection 2869B* data collector.

The inserts were put into a four-cavity steel mold housing. During injection molding, three of the four cavities were plugged by metal inserts and only one was used for the mold insert shown in Fig. 1. Fig. 2 shows the movable half of the mold, the ejection system and the arrangement of the inserts.

2.2. Materials

The 3D printed mold inserts used for injection molding were produced with the *PolyJet* technology (*Objet Alaris 30, Objet Geometries Ltd.*). The material was an epoxy-acrylate with the commercial name *FullCure 720*. The material is manufactured by *Stratasys Ltd.* and its properties are shown in Table 1.

The parts were injection molded from a homo-polypropylene; its commercial name is *Tipplen H145 F*. It was purchased from *MOL Group Public Limited Company* (Hungary). The relevant properties of the material can be seen in Table 2.

3. Development of a state monitoring method for 3D printed mold inserts

We assumed that deformation of the mold insert has two main causes. The first is thermal expansion due to the elevated temperatures during injection molding. The second is mechanical deformation, mainly caused by cavity pressure. We measured the magnitude of thermal expansion before injection molding, and called this measurement thermal calibration.

3.1. Thermal calibration and preliminary experiments

A mold insert has two main load during injection molding. The first is the mechanical (clamping, cavity pressure etc.) and the second is the thermal load. As we measure the deformation of the mold insert, the thermal expansion, caused by the thermal load plays an important role in the evaluation. On the other hand, the polymeric mold insert has an order of magnitude higher thermal expansion than that of a steel insert. During the thermal calibration, our goal was to show the effect of the insert temperature on the measured deformation.

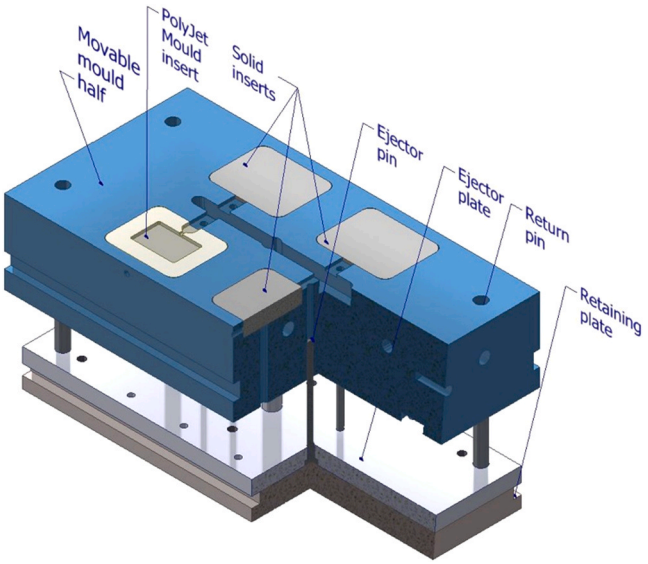

Fig. 2. The movable half of the mold housing, the ejection system and the inserts.

Table 1
The physical properties of *Stratasys FullCure 720*.

Physical properties	Unit	Typical value
Tensile strength	MPa	50 – 65
Elongation at break	%	15 – 25
Modulus of elasticity	GPa	2 – 3
Shore hardness (D scale)	–	83–86
Heat deflection temperature (HDT) (0.45 MPa)	°C	45–50
Glass transition temperature	°C	48–50
Rockwell hardness (M scale)	–	73–76

Table 2
The typical physical properties of *Tipplen H145F*.

Physical properties	Unit	Typical value
Melt flow rate (MFR) (230 °C / 2.16 kg)	g/10 min	29
Flexural modulus	GPa	1.8
Module of elasticity (in tension)	GPa	1.99
Tensile stress at yield	MPa	39
Tensile strain at yield	%	9
Recommended processing temperature	°C	190–235

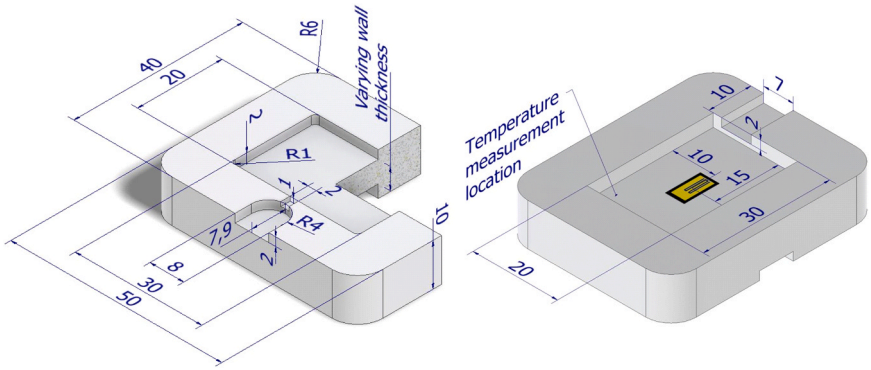

Fig. 1. The mold insert and the position of the strain gauge at the back of it. (All the dimensions are in mm).

Before thermal calibration, the strain gauges were glued to the back of the mold inserts, as shown on the right hand side of Fig. 1. Then, an *Ahlborn Almemo NiCr-Ni T 190–0* thermocouple was placed right next to the strain gauge to measure the temperature of the insert. Fixing of the thermocouple was done using a heat resistant glue. The thermocouple was connected to an *Ahlborn Almemo 8990–6* data collector unit. The inserts were placed inside the mold and then the assembly was put into a *Faithful WGLL-125 BE* drying oven for controlled heating, and thermal calibration was carried out on the inserts that were later used for injection molding. The wall thicknesses of these inserts were 4 mm, 5 mm and 6 mm. The explanation of varying wall thickness can be seen on the left hand side of Fig. 1.

During the heating of the inserts, the signals of the strain gauge and the thermocouple were recorded. Strain is shown as a function of temperature in the thermal calibration diagram, in Fig. 3. It is clear that strain shows a nearly linear relationship to temperature up to the value of approximately 45 °C. The presence of this threshold temperature is most likely caused by that the inserts reach the maximal volume of the metal mold cavity and therefore cannot expand any further.

Fig. 3 shows that the maximal strain caused by thermal expansion is in the range of 0.15 – 0.17%. In each injection molding cycle, the temperature and the strain of the mold inserts were measured in real time for in-situ monitoring of deformation and the operational temperature range. Another important goal was to keep the temperature below Tg to prevent early failure of the inserts. A significant benefit of the temperature measurement was that the necessary delay times between injection molding cycles could be determined. By keeping sufficient cooling time and delay time between the cycles, the maximum insert temperature at the back was 30–35 °C and the alteration of the insert temperature was only 5–10 °C. Based on these results, the thermal load only had a minor effect on the measured strain.

3.2. Filling tests and preparation for the injection molding series

After thermal calibration, a series of injection molding tests were carried out with the inserts with three different wall thicknesses (4 mm, 5 mm and 6 mm). First, we performed a mold filling test to find the necessary maximum injection pressures for different short shots. The characteristic points of filling and the corresponding maximum injection pressures can be seen in Fig. 4(a) and (b), respectively.

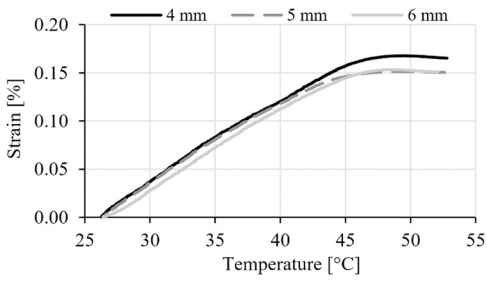

Fig. 3. The thermal calibration diagram of the mold inserts.

After the mold filling test, we performed injection moldings with the 6 mm wall insert. We used an Arburg Allrounder Advance 270S 400–170 injection molding machine (ARBURG GmbH) with a screw diameter of 30 mm. The default parameters were a clamping force of 10 tons, an injection rate of 10 cm^3/s, an injection pressure limit of 300 bars, a volume of 25 cm^3, a decompression volume of 4 cm^3 and a residual cooling time of 35 s.

We used the first three injection molding cycles to find the proper switchover point from the filling to the holding phase. The injected volume and the holding pressure data for these three preliminary experiments can be found in the first three rows of Table 3. The volume of the injected polymer melt was gradually increased after each cycle and the strains and the temperatures were measured during the three injection molding cycles. These strain and temperature results are presented in Fig. 5. Maximum strain grew after each cycle because the injected polymer melt volume was increased by changing the switchover point. The results indicate that after each injection molding cycle, residual strain gradually increased. This is possibly caused by the repeated injection pressure and the clamping force that deforms the mold insert in each cycle. The other source of the increasing residual strain is the gradual heating of the mold inserts by the hot polymer melt and the tempered movable mold half. The measured temperature increases faster during and right after the third injection molding cycle because in that moment the hot polymer melt reaches the thermocouple position. As can be seen from the results presented in Fig. 5, the temperature of the mold insert increases from the initial 26 °C to the 31 °C maximum, after the third injection molding cycle. The effect of temperature on the strain of the mold insert was demonstrated in Fig. 3. Based on this and the temperature range of the first three injection molding cycles, strain caused by thermal expansion is approximately 0.03–0.05%, depending on the wall thickness of the insert. The benefit of this is that strain caused by thermal expansion can be estimated in the operating temperature range. After the third injection molding cycle, the insert cools down. Due to the viscoelastic behavior of the polymeric materials, the residual strain gradually decreases as well, after unloading the system.

After finding the proper switchover point, we continued injection molding with the 6 mm wall insert. The main processing parameters for these cycles are in rows 4–9 of Table 3. The insert was usable for nine cycles altogether and the holding pressure was changed in two-cycle steps from the fourth to the ninth injection molding cycles. During the eighth and ninth cycle, the increased holding pressure required a greater clamping force in order to prevent unwanted mold opening, therefore the default clamping force was increased. The higher mechanical loads accelerated the fracture of the mold insert.

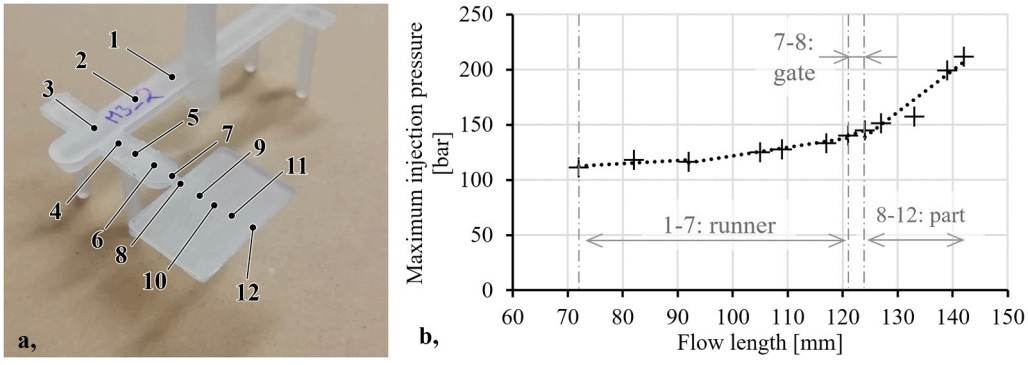

Fig. 4. The characteristic points of the filling test (a) and the corresponding maximum injection pressures (b).

Table 3
The parameter sets of the injection molding series in the case of the 6 mm thick insert.

Cycle number –	Injected volume [cm^3]	Holding pressure [bar]	Holding time [s]	Clamping force [ton]	Note
1	7	0	10	10	Preliminary experiment
2	8	0	10	10	Preliminary experiment
3	10	0	10	10	Preliminary experiment
4	10.5	150	10	10	–
5	10.5	150	10	10	–
6	10.5	75	10	10	–
7	10.5	75	10	10	–
8	10.5	200	10	20	–
9	10.5	200	10	20	Insert cracked

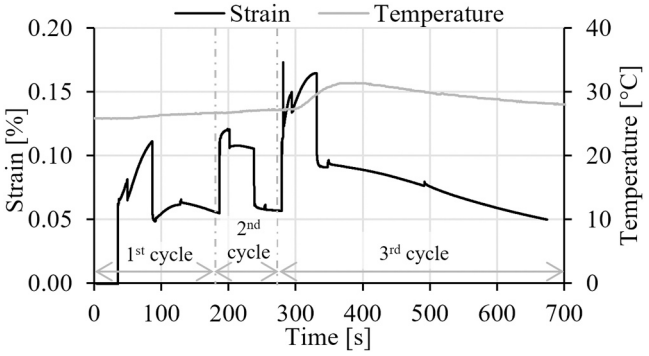

Fig. 5. The strain–time and temperature-time diagram of the first three injection molding cycles in the case of the 6 mm thick insert.

3.3. Pressure and strain results of the injection molding series

The strain, as a function of time in the fourth and fifth cycles is presented in Fig. 6(a), and the explanation of each segment of the strain curve is shown in Fig. 6(b). There is an instantaneous increase in strain during the filling phase, which is followed by a lower gradient increase during the holding phase. In the holding phase of the fourth cycle, the maximum of the strain reached 1.13%. As residual cooling time begins, strain converges to a constant level at roughly 0.75%. From this level, strain drops as the mold opens and the part is removed. However, after the cycle is finished, the strain converges to the non-zero level of roughly 0.17% in the fourth cycle, indicating a residual strain after the cycle is finished. The fifth cycle starts from this residual strain and shows a similar characteristic. The maximal strain in this cycle is around 1.38% and the residual strain level increases compared to the end of the fourth cycle.

As can be seen from the results of Figs. 5 and 6, the residual strain increases after each injection molding cycle. Therefore, the maximum of relative strain, caused by cavity pressure, was introduced for each injection molding cycle, and can be calculated with Eq. (1):

$$\varepsilon_{max,rel,i} = \varepsilon_{max,abs,i} - \varepsilon_{res,i-1} \quad (1)$$

Where $\varepsilon_{max,rel,i}$ is the maximum of relative strain in the ith cycle, $\varepsilon_{max,abs,i}$ is the maximum of absolute strain in the ith cycle and $\varepsilon_{res,i-1}$ is the residual strain after the (i−1)th cycle.

The cavity pressure and the absolute strain curves of the fourth and the fifth injection molding cycles are presented in Fig. 7. The results indicate that the curves are similar. The maximum of the absolute strain curves occur delayed in time relative to the maximum of the cavity pressure curves. This phenomenon is caused by the viscoelastic behavior of the polymer inserts. Residual strain can also be observed at the beginning of the fifth cycle.

Residual strain gradually increased and during the ninth cycle, the mold insert broke. The residual strain, the maximum values of absolute strain and relative strain (calculated according to (1)), and the maximums of cavity pressure are shown in Table 4.

The strain and cavity pressure measurement method shown above can be used for the in-situ and real-time state monitoring of inserts because mechanical failure leads to an immediate and sharp change in both the cavity pressure curve and the absolute strain curve. The

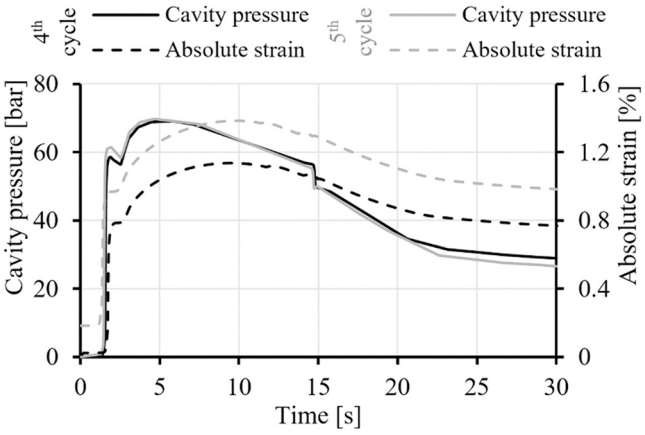

Fig. 7. The cavity pressure–time and the absolute strain–time diagrams of the fourth and fifth injection molding cycles in the case of 6 mm thick insert.

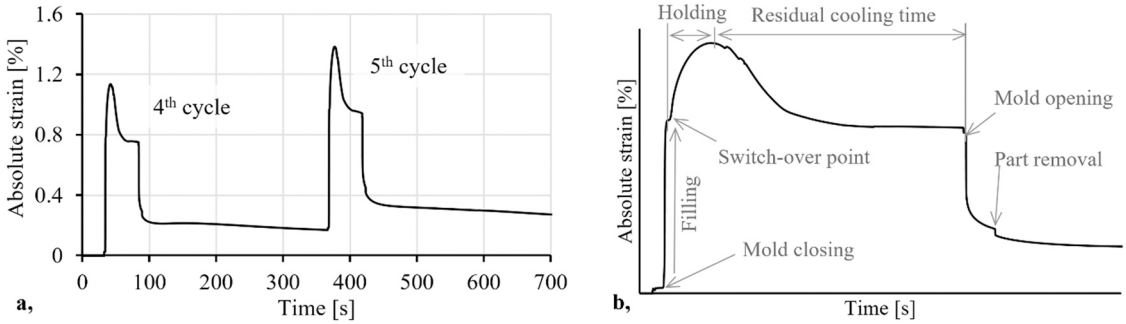

Fig. 6. The strain–time diagram of the fourth and fifth injection molding cycles in the case of the 6 mm thick insert (a) and the explanation of each segment (b).

Table 4
The maximums of the strain and cavity pressure of the 4th–9th injection molding cycles in the case of the 6 mm thick insert.

Cycle number -	Maximum of absolute strain %	Maximum of relative strain %	Residual strain %	Cavity pressure maximum Bar	Note
4	1.14	1.14	0	69.1	–
5	1.38	1.21	0.17	69.7	–
6	0.98	0.72	0.26	55.5	–
7	0.90	0.64	0.26	54.9	–
8	1.20	0.96	0.24	58.2	Part with flash
9	0.95	0.68	0.27	98.4	Insert broke

practical relevance of this monitoring method from an industrial aspect is significant as it can immediately indicate mold insert failure. This monitoring method is able to function as an active injection molding process controller. The measured cavity pressure and absolute strain curves in the ninth injection molding cycle of the 6 mm thick walled insert can be seen in Fig. 8.

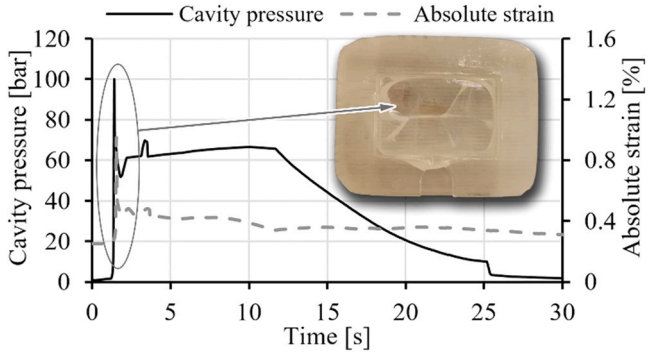

Fig. 8. The cavity pressure–time and the absolute strain–time diagrams of the 6 mm thick insert in the ninth injection molding cycle and the broke insert.

3.4. The correlational diagrams of the 6 mm, 5 mm and 4 mm thick inserts

We injection molded into all three prepared inserts. The holding pressure was changed between 0 bar and 125 bars in the case of the 4 mm wall insert. In the case of the 5 mm wall insert, the holding pressure was changed between 0 bar and 150 bars. The holding time was 10 s in all injection molding cycles. The 4 mm thick insert endured 11 cycles and broke in the 12th cycle, while the 5 mm thick insert endured 12 cycles and broke in the 13th cycle.

The maximums of the cavity pressure and the relative strain curves were measured and calculated, respectively, and used to characterize the stiffness of the mold inserts. These results are presented in Fig. 9 for the three different inserts. In the case of the 6 mm thick insert in Fig. 9 (c), the ninth measurement in Table 4 was left out of the diagram because of the mechanical failure of the insert, which made the maximums of relative strain and cavity pressure uncertain. The measurement point farthest from the fitted curve corresponds to the eighth data set in Table 4. In that case, the mold first opened, then the clamping force was

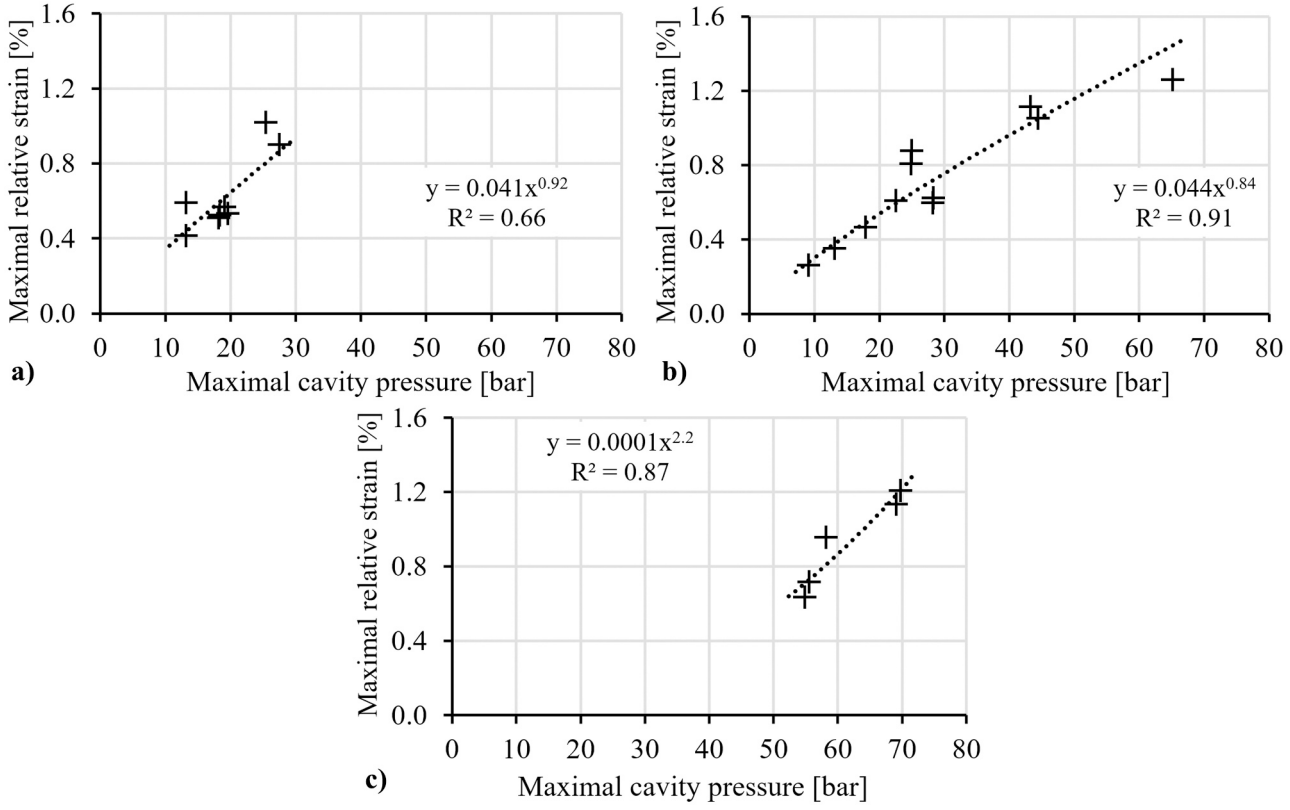

Fig. 9. The maximal relative strain–maximal cavity pressure diagrams for the 4 mm (a), 5 mm (b) and 6 mm (c) thick inserts.

increased to 20 tons, as it is presented in Table 3. It is quite probable that the high clamping force caused additional deformation to the mold insert, causing the deviation from the fitted curve. We injection molded into the 4 mm and 5 mm thick inserts as well. Maximal cavity pressure–maximal relative strain points for the 4 mm and 5 mm thick inserts can be seen in Fig. 9 (a) and (b), respectively.

The results of the three different inserts indicate a correlation between the increasing mechanical loads and the resulting increased maximal relative strain. This strain measurement can be used as an indirect cavity pressure monitoring method, after the necessary improvements. A future refinement of the presented method has to be the determination of the exact mathematical relation between maximal cavity pressure and maximal relative strain. A further advantage of the presented method is that the failure of the mold inserts can be predicted with adequate accuracy by measuring the accumulation of residual strain. The moment can be determined when the maximal allowed deformation is reached and the corresponding cavity pressure can be quantified. This method makes the in-situ state monitoring of mold inserts possible and local failures can be detected. The lifespan of the mold inserts can be improved as well by quantifying the necessary waiting time for the reduction of viscoelastic deformation.

4. Conclusion

In this paper, we performed a novel test series on 3D printed injection mold inserts. The inserts were made from an epoxy-acrylate and the material used for injection molding was a homo-polypropylene. We used a new method to examine the effects of thermal expansion on mold insert deformation. We placed the inserts into a four-cavity metal mold and then put the assembly in a drying oven for controlled tempering. During this time, the strain and temperature of the inserts were measured with a strain gauge and a thermocouple, respectively. This way, we determined the strain–temperature relationship of the inserts and were able to examine the effect of thermal expansion separately. Thermal calibration was used to estimate thermal strains in the operating temperature range of the inserts. We performed the thermal calibration of inserts with three different wall thicknesses: 4 mm, 5 mm and 6 mm.

After thermal calibration, we injection molded a series of parts with all the inserts. During injection molding, pressure was monitored directly in the cavity with a sensor and strain was measured with a strain gauge glued to the back of the insert. The 6 mm thick insert broke in the 9th cycle, the 5 mm thick insert in the 13th cycle, and the 4 mm thick insert in the 12th cycle. Residual strain after cycles showed an increasing tendency and the accumulation of these strains is a possible explanation for the failure of the inserts after only a few cycles. We recorded strain and cavity pressure during injection molding. Maximal strain occurred later than maximal cavity pressure. This is caused by the viscoelastic nature of the polymers. We calculated the relative strain maximum by subtracting the residual strain from the previous injection molding cycle from the maximum of the absolute strain of the current cycle. Maximum relative strains were compared to their respective maximum cavity pressures, and a correlational diagram was created for mold insert stiffness. These diagrams showed a correlation between the increased cavity pressures and the resulting increased maximal relative strains. In sum, we found a satisfactory correlation between the strain of the insert and cavity pressure. Further in-depth analysis and tests are necessary, and then this relationship can be utilized for in-situ monitoring of the state of the inserts during injection molding and predicting their mechanical failure. The necessary waiting time between injection molding cycles can also be determined, and this increases the lifespan of the inserts.

Funding

This work was supported by the National Research, Development and Innovation Office, Hungary (2019-1.1.1-PIACI-KFI-2019-00205, 2018-1.3.1-VKE-2018-00001, 2017-2.3.7-TÉT-IN-2017-00049, OTKA FK134336). The research reported in this paper and carried out at BME has been supported by the NRDI Fund (TKP2020 NC, Grant No. BME-NCS) based on the charter of bolster issued by the NRDI Office under the auspices of the Ministry for Innovation and Technology. This paper was supported by the János Bolyai Research Scholarship of the Hungarian Academy of Sciences. The research was supported by the ÚNKP-20-5 New National Excellence Program of the Ministry for Innovation and Technology from the source of the National Research, Development and Innovation Fund.

Declaration of Competing Interest

The authors declare that they have no known competing financial interests or personal relationships that could have appeared to influence the work reported in this paper.

Acknowledgements

We wish to thank ARBURG HUNGÁRIA KFT. for the ARBURG Allrounder 370S 700-290 injection molding machine, and TOOL-TEMP HUNGÁRIA KFT., LENZKES GMBH and PIOVAN HUNGARY KFT. for the accessories.

References

[1] M.-W. Wang, F. Arifin, V.-H. Vu, The study of optimal molding of a LED lens with grey relational analysis and molding simulation, Period. Polytech. Mech. Eng. 63 (2019) 278–294.
[2] Z. Keresztes, D. Pammer, J.P. Szabo, EBSD examination of argon ion bombarded Ti-6Al-4V samples produced with DMLS technology, Period. Polytech. Mech. Eng. 63 (2019) 195–200.
[3] J.G. Kovács, F. Szabó, N.K. Kovács, A. Suplicz, B. Zink, T. Tábi, H. Hargitai, Thermal simulations and measurements for rapid tool inserts in injection molding applications, Appl. Therm. Eng. 85 (2015) 44–51.
[4] B. Zink, J.G. Kovács, Enhancing thermal simulations for prototype molds, Period. Polytech. Mech. Eng. 62 (2018) 320–325.
[5] M.A. León-Cabezas, A. Martínez-García, F.J. Varela-Gandia, Innovative advances in additive manufactured moulds for short plastic injection series, Procedia Manuf. 13 (2017) 732–737.
[6] C. Whlean, Dr.C. Sheahan, Using additive manufacturing to produce injection moulds suitable for short series production, Procedia Manuf. 38 (2019) 60–68.
[7] A. Davoudinejad, M.R. Khosravani, D.B. Pedersen, G. Tosello, Influence of thermal ageing on the fracture and lifetime of additively manufactured mold inserts, Eng. Fail. Anal. 115 (2020), 104694.
[8] C.M. Cheah, C.K. Chua, H.S. Ong, Rapid moulding using epoxy tooling resin, Int. J. Adv. Manuf. Technol. 20 (2002) 368–374.
[9] B. Zink, N.K. Kovács, J.G. Kovács, Thermal analysis based method development for novel rapid tooling applications, Int. Commun. Heat. Mass Transf. 108 (2019), 104297.
[10] B. Zink, F. Szabó, I. Hatos, A. Suplicz, N.K. Kovács, H. Hargitai, T. Tábi, J. G. Kovács, Enhanced injection molding simulation of advanced injection molds, Polymers 9 (2017) 77.
[11] H.-S. Park, X.-P. Dang, Development of a smart plastic injection mold with conformal cooling channels, Procedia Manuf. 10 (2017) 48–59.
[12] H. Brooks, K. Brigden, Design of conformal cooling layers with self-supporting lattices for additively manufactured tooling, Addit. Manuf. 11 (2016) 16–22.
[13] K.M. Au, K.M. Yu, Conformal cooling channel design and CAE simulation for rapid blow mould, Int. J. Adv. Manuf. Technol. 66 (2013) 311–324.
[14] D. Tomasoni, S. Colosio, L. Giorleo, E. Ceretti, Design for additive manufacturing: thermoforming mold optimization via conformal cooling channel technology, Procedia Manuf. 47 (2020) 1117–1122.
[15] T. Wu, S.A. Jahan, Y. Zhang, J. Zhang, H. Elmounayri, A. Tovar, Design optimization of plastic injection tooling for additive manufacturing, Procedia Manuf. 10 (2017) 923–934.
[16] R. Boros, P. Kannan Rajamani, J.G. Kovács, Combination of 3D printing and injection molding: Overmolding and overprinting, Express Polym. Lett. 13 (2019) 889–897.
[17] H. Kalami, R.J. Urbanic, Design and fabrication of a low-volume, high-temperature injection mould leveraging a 'rapid tooling' approach, Int. J. Adv. Manuf. Technol. 105 (2019) 3797–3813.
[18] M. Vaezi, D. Safaeian, C.K. Chua, Gas turbine blade manufacturing by use of epoxy resin tooling and silicone rubber molding techniques, Rapid Prototyp. J. 17/2 (2011) 107–115.
[19] S. Jahan, T. Wu, Y. Shin, A. Tovar, H. El-Mounayri, Thermo-fluid topology optimization and experimental study of conformal cooling channels for 3D printed plastic injection molds, Procedia Manuf. 34 (2019) 631–639.

[20] N. Hopkinson, P. Dickens, A comparison between stereolitography and aluminium injection moulding tooling, Rapid Prototyp. J. Volume 6 (Number 4) (2000) 253–258.
[21] G.A. Mendible, J.A. Rulander, S.P. Johnston, Comparative study of rapid and conventional tooling for plastics injection molding, Rapid Prototyp. J. 23/2 (2017) 344–352.
[22] A. Kampker, J. Triebs, S. Kawollek, P. Ayvazand, T. Beyer, Direct polymer additive tooling – effect of additive manufactured polymer tools on part material properties for injection moulding, Rapid Prototyp. J. 25/10 (2019) 1575–1584.
[23] T. Tábi, N.K. Kovács, I.E. Sajó, T. Czigány, S. Hajba, J.G. Kovács, Comparison of thermal, mechanical and thermomechanical properties of poly(lactic acid) injection-molded into epoxy-based Rapid Prototyped (PolyJet) and conventional steel mold, J Therm Anal Calorim 123 (2016) 349–361.
[24] P.G. Martinho, P.J. Bártolo, A.S. Pouzada, Hybrid moulds: effect of the moulding blocks on the morphology and dimensional properties, Rapid Prototyp. J. 15/1 (2009) 71–82.
[25] R.A. Harris, H.A. Newlyn, R.J.M. Hague, P.M. Dickens, Part shrinkage anomilies from stereolitography injection mould tooling, Int. J. Mach. Tools Manuf. 43 (2003) 879–887.